Research Article

Hu Liu, Yu Jiang*, Anqi Lang, Yajie Wang, Xiaoduan Zou, Jinsong Ping, Yutong Chang, Yongzhang Yang, Chen Zheng, Yi Lian, and Jianfeng Cao

Analysis of the equilibrium points and orbits stability for the asteroid 93 Minerva

https://doi.org/10.1515/astro-2022-0207
received June 30, 2022; accepted October 13, 2022

Abstract: In this article, we study the orbital dynamics with the gravitational potential of the asteroid 93 Minerva using an irregular shape model from observations. We calculate its physical size, physical mass, surface height, and zero-velocity surface. Meanwhile, we recognize that there are five equilibrium points around Minerva, four of which are external, and one is internal. Two of the external equilibrium points are stable and near the y-axis, while two external equilibrium points are unstable and near the x-axis. In addition, we study the changes in the number, position, and topological case of the equilibrium points when changing the spin speed and the density. We calculate the gravitational force acceleration of the polyhedron model, and we back up our calculations by simulating the orbit of one moonlet under the gravitational force acceleration of Minerva. With the simulation result, we demonstrate the existence of stable orbits around Minerva.

Keywords: asteroids, 93 Minerva, equilibrium points

1 Introduction

Asteroids have extremely high scientific exploration value. Through research and exploration of asteroids, we can further utilize space resources and verify asteroid defense technologies. Since the Galileo spacecraft flew by the 951 Gaspra mission in 1991 (Belton *et al*. 1992), the exploration of asteroids and comets has come into the spotlight. A number of countries or organizations in the world have completed asteroid visited missions. In 1997, the NEARS (Near Earth Asteroid Rendezvous Shoemaker) probe launched by NASA (National Aeronautics and Space Administration) completed the visit of asteroids such as the asteroid 253 Mathilde (Veverka *et al*. 1997, 2000). In 2003, JAXA (Japan Aerospace Exploration Agency) launched The Hayabusa probe that visited the asteroid 25143 Itokawa and returned, and this is the first time for humans to obtain a sample of an asteroid (Fujiwara *et al*. 2006, Abe *et al*. 2006). In 2004, the Rosetta spacecraft of ESA (European Space Agency) imaged the comet 67P/Churyumov-Gerasimenko and leap past the asteroid 21 Luteria with a distance of 3,160 km (Barucci *et al*. 2007). In 2012, the Chang'e 2 satellite of CNSA (China National Space Administration) conducted a flyby of 4179 Toutatis asteroid at a distance of 3.2 km (Huang *et al*. 2013, Zhao *et al*. 2013, Ji *et al*. 2015, Zou *et al*. 2014) and obtained high-definition images of its surface, as shown in Figure 1. In the future, more asteroid exploration missions will be gradually carried out, and become an indispensable step in deep space exploration.

* **Corresponding author: Yu Jiang,** State Key Laboratory of Astronautic Dynamics, Xi'an Satellite Control Center, Xi'an, 710043, China, e-mail: jiangyu_xian_china@163.com
Hu Liu: State Key Laboratory for Strength and Vibration of Mechanical Structures, School of Aerospace Engineering, Xi'an Jiaotong University, Xi'an 710049, Shaanxi, China; Key Laboratory for Fault Diagnosis and Maintenance of Spacecraftin-Orbit, Xi'an Satellite Control Center, Xi'an, 710043, China
Anqi Lang: State Key Laboratory for Strength and Vibration of Mechanical Structures, School of Aerospace Engineering, Xi'an Jiaotong University, Xi'an 710049, Shaanxi, China
Yajie Wang: Key Laboratory for Fault Diagnosis and Maintenance of Spacecraftin-Orbit, Xi'an Satellite Control Center, Xi'an, 710043, China
Xiaoduan Zou: Planetary Science Institute, Tucson, 85719, United States
Jinsong Ping: National Astronomical Observatories, Chinese Academy of Sciences, Beijing, 100012, China
Yutong Chang: State Key Laboratory of Astronautic Dynamics, Xi'an Satellite Control Center, Xi'an, 710043, China
Yongzhang Yang: Yunnan Observatories, Chinese Academy of Sciences, Kunming, 650216, China
Chen Zheng: School of Mathematics and Statistics, Henan University, Kaifeng, Henan, 475004, China
Yi Lian: National Astronomical Observatories, Chinese Academy of Sciences, Beijing, 100012, China; College of Geographic and Environmental Sciences, Tianjin Normal University, Tianjin, 300387, China
Jianfeng Cao: Aerospace Flight Dynamics Laboratory Beijing Aerospace Control Center Science and Technology, Beijing, 100094, China

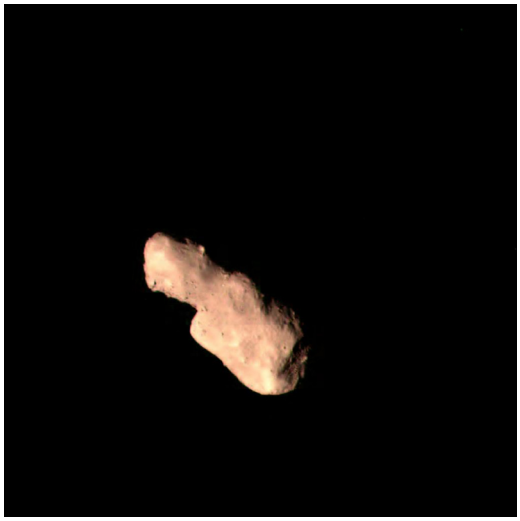

Figure 1: Image of Toutatis by Chang'e 2 engineering camera designed to monitor the state of the solar panel on December 13th, 2012.

Considering the need for asteroid exploration in the solar system, it is of great significance to study the orbital environment around asteroids. Werner and Scheeres (1996) proposed a polyhedral model method to calculate the gravitational force of irregularly shaped asteroids, which was later widely used in the model building of the gravitational field environment of asteroids. Scheeres *et al.* (1996) applied the Jacobian integral of particles orbiting around asteroids. With the Jacobian integral, we can determine the range of particle motion on the zero-velocity surface. From a practical point of view, it is an important way to understand the orbital dynamics near asteroid by studying the equilibrium points and periodic orbits around an asteroid, and it is also the key to deep space exploration orbits designing. Jiang *et al.* (2014) proposed a theory of local dynamics around the equilibrium points and classified nondegenerate equilibrium points into different cases. Wang *et al.* (2014) used the classification proposed by Jiang *et al.* (2014) to calculate the stability and the topological classification of equilibrium points around 23 asteroids. Yu and Baoyin (2012a) divided the periodic orbits near the equilibrium point in the gravitational field into several topological cases, and then gave a complete classification of periodic orbits. Previous studies have used polyhedral models to analyze the dynamic environment around asteroids, such as 21 Lutetia, 41 Daphne, and 624 Hektor (Mota *et al.* 2019, Jiang 2018, 2019, Jiang *et al.* 2018, Moura *et al.* 2020, Aljbaae *et al.* 2019). Our goal is to analyze the dynamic environment around binary or triple asteroid systems with large mass ratios, considering the gravitational potential generated by their irregular shapes.

Asteroid 93 Minerva is the fifth triple asteroid system to be discovered, located in the main belt (r = 2.75 au) (Marchis *et al.* 2009). It is a large and dark C-type asteroid (Lazzaro *et al.* 2004). The shape of Minerva is almost spherical, its equivalent diameter is nearly 154 km, and the rotation period is 5.981767 ± 0.000004 h (Marchis *et al.* 2013). It has two small moonlets Aegis and Gorgoneion, the approximate diameters of the two moonlets are 3.6 ± 1.0 and 3.2 ± 0.9 km, and the orbital semi-major axes are 623.5 and 375 km (Marchis *et al.* 2013). Minerva is such a typical triple asteroid system, and there are a lot of papers studying its physical properties on it (Tedesco *et al.* 2002, Price *et al.* 2001, Usui *et al.* 2011). However, few articles analyzed the Minerva system dynamics. In this article, we investigate the Minerva system dynamics, which is both interesting and important for our study. Our research will make a contribution to understand the dynamical behavior of massless particles in a triple asteroid system.

In Section 2, we discuss the physical properties of 93 Minerva, including its physical shape, physical size, and surface height. In addition, we calculate the equilibrium points, zero-velocity surfaces, equilibrium points eigenvalues, and their corresponding topological cases. In Section 3, we analyze the changes in the equilibrium points when the spin speed and the density of the asteroid change. When the spin speed is gradually increased to 2.42 times, it is found that the number of equilibrium points will first increase and then decrease. When the density changes, the topological cases of the equilibrium points also changes, which means the stability changes. Section 4 presents the simulation of the moonlet orbits under the Minerva gravitational potential. The gravitational potential of Minerva was calculated by using the polyhedron model and observational data. Section 5 briefly reviews the findings of the study.

2 Equations of motion and equilibrium points

In this section, we first built the three-dimensional model of Minerva and calculated the physical size, physical mass, and surface height. Then, we discussed the equations of motion, the equilibrium points, and eigenvalues of the equilibrium points around a uniformly rotating object, and calculated the equilibrium points and their eigenvalues of Minerva. Then we analyzed the stability of the equilibrium points.

2.1 Physical model

Since the gravity ratio of the two moonlets to the main asteroid is too small and the distance from the main asteroid is too far, we ignored moonlets gravity when calculating the equilibrium points. We used the polyhedral model method for calculations (Werner and Scheeres 1996), and this model of the asteroid Minerva contains 402 vertices and 800 triangular faces (Marchis *et al.* 2013).

We translate and rotate the model of the asteroid. The centroid of the asteroid coincides with the origin of the coordinate system. The axes x, y, and z coincide, in this order, with the axes of the lowest moment of inertia, the intermediate moment of inertia, and that of the greatest moment of inertia (Jiang and Liu 2019).

The bulk density of Minerva is estimated to be $\rho = 1.75 \pm 0.30$ g cm^{-3}, and the rotation period is estimated to $T = 5.981767 \pm 0.000004h$ (Marchis *et al.* 2013). And we used $\rho = 1.75$ g cm^{-3} and $T = 5.982h$ in our calculation. Figure 2 shows the 3D polyhedron model of the asteroid Minerva. The physical size of Minerva model is calculated to be 182.96 km × 164.37 km × 143.79 km, and the total mass of the model is 3.3603×10^{18} kg. The moment of inertia is expressed as follows:

$$I_{xx} = 7.3735 \times 10^{12} \text{ kg km}^2$$
$$I_{yy} = 8.0672 \times 10^{12} \text{ kg km}^2$$
$$I_{zz} = 9.2386 \times 10^{12} \text{ kg km}^2.$$

Surface height refers to the distance between the centroid of the asteroid and a point on the surface with a fixed latitude and longitude. By performing calculations on the polyhedral model, we obtained the surface height data for Minerva, as shown in Figure 3. From the surface height data, we can see that the value range of the surface height is 63.7–93.1 km, and the average value is about 74.4 km. At the same time, the ratio of the maximum to the minimum surface height is about 1.5, which is much smaller than most asteroids. In addition, we can see from the contour map significantly that there are four convex areas and six concave areas on the surface of the asteroid, and these irregular areas made a contribution to the uneven gravity of Minerva.

2.2 Calculation of equilibrium points

We calculated the equilibrium points and zero-velocity surface in the asteroid's gravitational potential. When massless particles move in an asteroid's gravitational potential, we can describe its equation of motion in Cartesian coordinates. The spin speed of the asteroid is $\boldsymbol{\omega}$. The vector from the centroid of the asteroid to the particle is $\boldsymbol{r}(x, y, z)$. The Newtonian form of the kinetic equation for the motion of the particle relative to the asteroid can be expressed as (Jiang *et al.* 2014):

$$\ddot{\boldsymbol{r}} + 2\boldsymbol{\omega} \times \dot{\boldsymbol{r}} + \boldsymbol{\omega} \times (\boldsymbol{\omega} \times \boldsymbol{r}) + \dot{\boldsymbol{\omega}} \times \boldsymbol{r} + \frac{\partial U(\boldsymbol{r})}{\partial \boldsymbol{r}} = 0. \quad (1)$$

The gravitational potential U and gravitational acceleration ∇U of the asteroid can be calculated by the polyhedron model method (Werner and Scheeres 1996).

$$U = -\frac{1}{2} G\sigma \sum_{e \in \text{edges}} \boldsymbol{r}_e \cdot \mathbf{E}_e \cdot \boldsymbol{r}_e \cdot L_e + \frac{1}{2} G\sigma \sum_{f \in \text{faces}} \boldsymbol{r}_f \cdot \mathbf{F}_f \cdot \boldsymbol{r}_f \cdot \omega_f \quad (2)$$

$$\nabla U = G\sigma \sum_{e \in \text{edges}} \mathbf{E}_e \cdot \boldsymbol{r}_e \cdot L_e - G\sigma \sum_{f \in \text{faces}} \mathbf{F}_f \cdot \boldsymbol{r}_f \cdot \omega_f. \quad (3)$$

Among them, $G = 6.67 \times 10^{-11} \text{m}^3 \text{ kg}^{-1} \text{ s}^{-2}$ is the Newton's gravitational constant, which σ is the bulk density of the asteroid, $\mathbf{r}_e$ and $\mathbf{r}_f$ are the position vectors of the polyhedral model related to the edges and faces, $\mathbf{E}_e$ is the dyad of the polyhedral model calculated by two face and edge normal vectors of the polyhedral model, and $\mathbf{F}_f$ is the outer product of the surface normal vector, $\mathbf{L}_e$ is the integration factor of the particle, and ω_f means the signed solid angle of the face. We define the function H as follows:

$$H = \frac{1}{2}\dot{\boldsymbol{r}} \cdot \dot{\boldsymbol{r}} - \frac{1}{2}(\boldsymbol{\omega} \times \boldsymbol{r}) \cdot (\boldsymbol{\omega} \times \boldsymbol{r}) + U(\boldsymbol{r}). \quad (4)$$

We can see from this equation, if $\boldsymbol{\omega}$ is constant, then H is also constant, which is called the Jacobi function; otherwise, it is called the Jacobi integral. The physical meaning of the Jacobian integral is the relative energy of particles. Meanwhile, the effective potential $V(\boldsymbol{r})$ is defined as follows:

$$V(\boldsymbol{r}) = -\frac{1}{2}(\boldsymbol{\omega} \times \boldsymbol{r}) \cdot (\boldsymbol{\omega} \times \boldsymbol{r}) + U(\boldsymbol{r}). \quad (5)$$

Substituting it into Eq. (1), we can obtain

$$\ddot{\boldsymbol{r}} + 2\boldsymbol{\omega} \times \dot{\boldsymbol{r}} + \dot{\boldsymbol{\omega}} \times \boldsymbol{r} + \frac{\partial V(\boldsymbol{r})}{\partial \boldsymbol{r}} = 0. \quad (6)$$

For asteroids with uniform spin, the aforementioned formula can be simplified to

$$\ddot{\boldsymbol{r}} + 2\boldsymbol{\omega} \times \dot{\boldsymbol{r}} + \frac{\partial V(\boldsymbol{r})}{\partial \boldsymbol{r}} = 0. \quad (7)$$

At the same time, the Jacobi function can be expressed by the effective potential as follows:

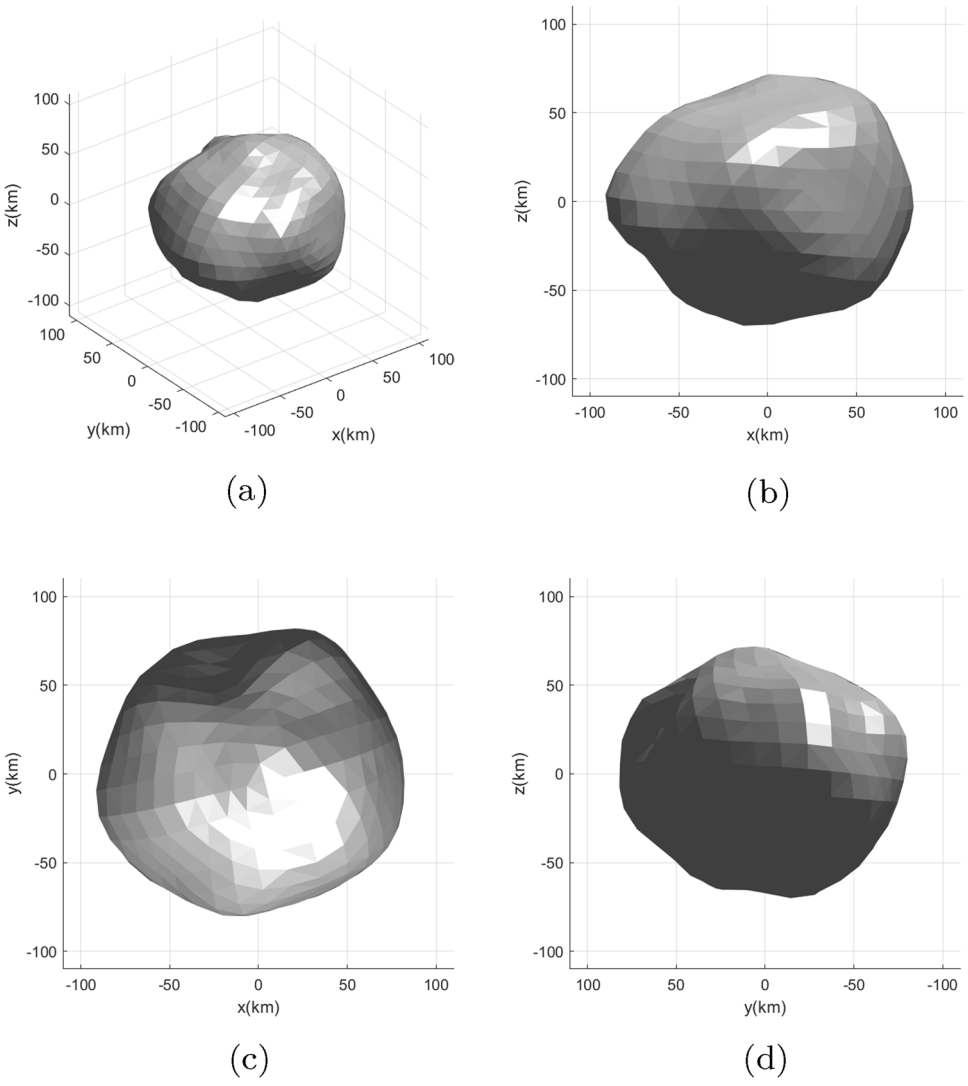

Figure 2: The polyhedron model of asteroid Minerva consists 402 vertices and 800 triangular faces in total. (a) 3D view. (b) $+y$ viewing angle. (c) $+z$ viewing angle. (d) $+x$ viewing angle.

$$H = \frac{1}{2}\dot{\boldsymbol{r}} \cdot \dot{\boldsymbol{r}} + V(\boldsymbol{r}). \tag{8}$$

The zero-velocity surface is an important concept when studying the particle motion interval, and it can be defined by the following equation (Scheeres *et al.* 1996, Yu and Baoyin 2012b):

$$V(\boldsymbol{r}) = H. \tag{9}$$

The equilibrium points are the critical points of the effective potential $V(\boldsymbol{r})$. The relative equilibrium points in the gravitational potential of a uniformly rotating asteroid means that if the particles are located at the relative equilibrium point, the resultant force of the particles is zero. So, the positions of the equilibrium points in the potential energy of the asteroid can be calculated by the following equation (Jiang *et al.* 2014):

$$\frac{\partial V(x,y,z)}{\partial x} = \frac{\partial V(x,y,z)}{\partial y} = \frac{\partial V(x,y,z)}{\partial z} = 0. \tag{10}$$

The equilibrium points information of Minerva is shown in Table 1. From Table 1, we found that the equilibrium points are not on the equatorial plane, because Minerva is not north-south symmetry. The positions of the equilibrium points in space are shown in Figure 4(a), and they are approximately evenly distributed around Minerva. The zero-velocity surfaces and projections of equilibrium points in the $+z$ view are shown in Figure 4(b), and the gray part is the projection of the asteroid.

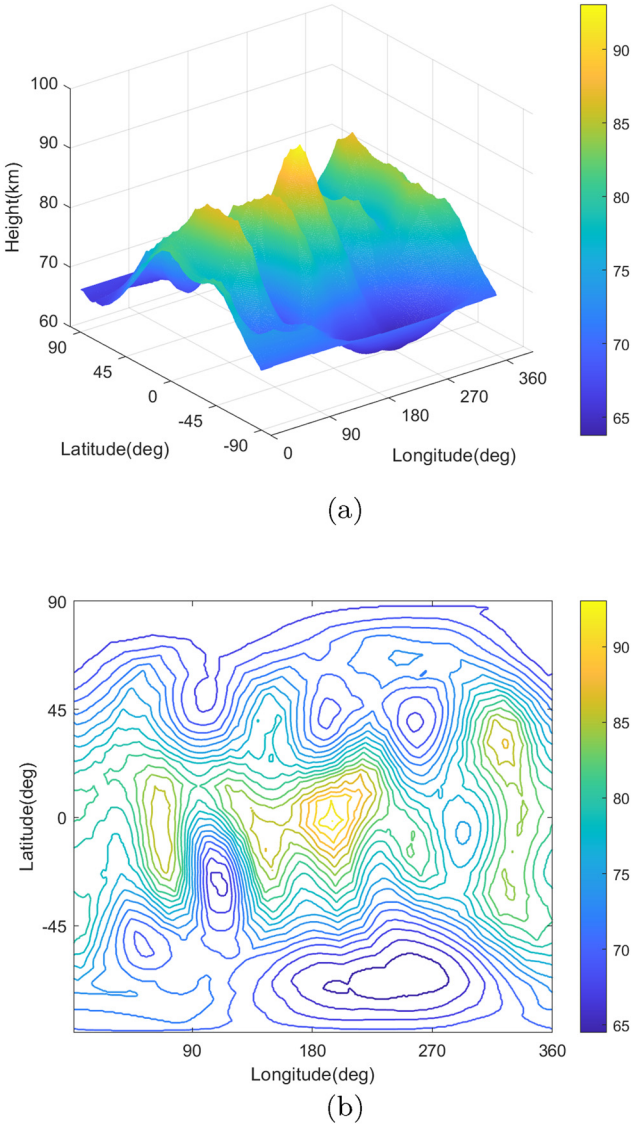

Figure 3: Surface height of Minerva, and the units on the colorbar are km. (a) 3D plot and (b) contour plot.

2.3 Eigenvalues of equilibrium points

Denote point (x_L, y_L, z_L) as an equilibrium point and point (x, y, z) as a point near the equilibrium point. λ represents the eigenvalue of the equilibrium point. Then λ could be calculated by the following formula (Jiang *et al.* 2014), in which $V_{pq} = \left(\frac{\partial^2 V}{\partial p \partial q}\right)_L$.

$$\begin{aligned}\lambda^6 &+ (V_{xx} + V_{yy} + V_{zz} + 4\omega^2)\lambda^4 \\ &+ (V_{xx}V_{yy} + V_{xx}V_{zz} + V_{yy}V_{zz} - V_{xy}^2 - V_{xz}^2 - V_{yz}^2 \\ &+ 4\omega^2 V_{zz})\lambda^2 + (V_{xx}V_{yy}V_{zz} + 2V_{xy}V_{xz}V_{yz} - V_{xx}V_{yz}^2 \\ &- V_{yy}V_{xz}^2 - V_{zz}V_{xy}^2) = 0.\end{aligned} \tag{11}$$

Table 1: Positions of the equilibrium points around Minerva

Equilibrium points	x (km)	y (km)	z (km)
E1	133.582	−43.1355	−3.17847
E2	−28.4497	135.744	−0.659530
E3	−139.975	−22.1477	0.398907
E4	3.48440	−138.232	0.266672
E5	0.533699	−1.45692	−6.71972

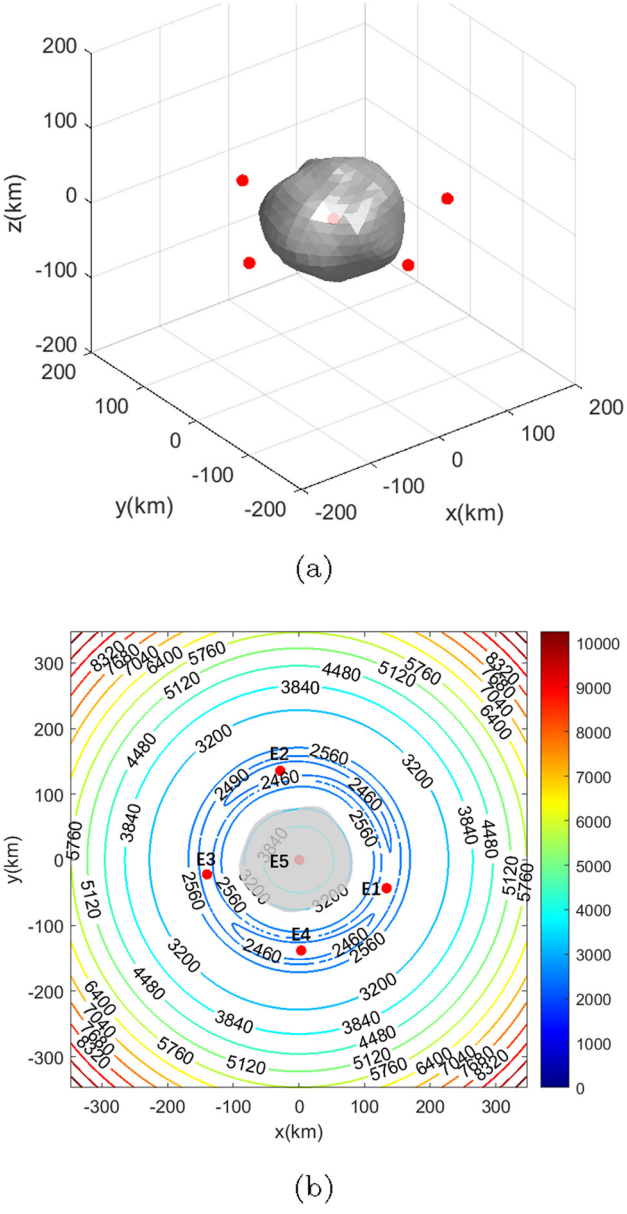

Figure 4: Locations of the equilibrium points of asteroid Minerva. (a) The positions of the equilibrium points in space. (b) Zero-velocity curves and projections of the equilibrium points in the $+z$ view.

Table 2: Eigenvalues of the equilibrium points around Minerva

Equilibrium points	λ_1	λ_2	λ_3	λ_4	λ_5	λ_6
E1	0.300882i	−0.300882i	0.298503i	−0.298503i	0.096861	−0.096861
E2	0.301989i	−0.301989i	0.243215i	−0.243215i	0.141071i	−0.141071i
E3	0.311381i	−0.311381i	0.294989i	−0.294989i	0.117155	−0.117155
E4	0.299099i	−0.299099i	0.255565i	−0.255565i	0.124411i	−0.124411i
E5	0.963082i	−0.963082i	0.753216i	−0.753216i	0.378339i	−0.378339i

The detailed calculation process is in Appendix A. The calculated eigenvalues of the asteroid Minerva are presented in Table 2.

The topological cases of the equilibrium points can be determined by the following distributions of eigenvalues shown in Table 3 (Jiang *et al*. 2014, Wang *et al*. 2014), case 1 is stable, and other cases are unstable. From Table 3, we can see that E1 and E3 belong to case 2, and E2, E4, and E5 belong to case 1. Therefore, among the five equilibrium points of Minerva, E2, E4, and E5 are linearly stable equilibrium points, and E1 and E3 are unstable equilibrium points.

3 Changes of equilibrium points during the variety of parameters

When we change the parameters of the asteroid, its gravitational field and dynamics environment also change. For equilibrium points, bifurcations and annihilation may occur (Jiang and Baoyin 2018). We analyze the influences on the equilibrium points of Minerva by changing the spin speed and density.

3.1 The change of spin speed

We observed the movement of the equilibrium point positions when the spin speed ω changed, and we defined the initial spin speed $\omega_0 = 2\pi / T$. Figure 4(b) shows the positions of the equilibrium points at the initial spin speed ω_0. We kept the density unchanged, gradually increased the spin speed from $0.5\omega_0$ to $2.42\omega_0$, and observed the change of the equilibrium points. Some typical results are shown in Figure 5.

As Figure 5 shows, when the spin speed changes, the number and positions of the equilibrium points also change gradually. When $\omega = 0.5\omega_0$, the number of equilibrium points is five, and four external equilibrium points positions are located close to 200 km from the centroid of the asteroid. The distance is far away than that when $\omega = 1.0\omega_0$, whose distance is about 150 km. As the spin speed varies more than $1.0\omega_0$, the creation and annihilation of five equilibrium points of Minerva appear. When ω increases from $1.06\omega_0$ to $1.07\omega_0$, the number of equilibrium points will change from five to seven, and the two newly created equilibrium points E6 and E7 almost overlap. As ω increases to $2.0\omega_0$ continually, the two newly created equilibrium points will gradually separate, and all the external equilibrium points

Table 3: Topological classification of equilibrium points in the gravitational potentials of asteroids

Topological cases	Eigenvalues	Stability
Case 1	$\pm i\beta_j (\beta_j \in \mathbb{R}, \beta_j > 0, j = \{1, 2, 3\})$	Linearly stable
Case 2	$\alpha_j (\pm\alpha_j \in \mathbb{R}, \alpha_j > 0, j = 1), \pm i\beta_j (\beta_j \in \mathbb{R}, \beta_j > 0, j = \{1, 2\})$	Unstable
Case 3	$\alpha_j (\pm\alpha_j \in \mathbb{R}, \alpha_j > 0, j = \{1, 2\}), \pm i\beta_j (\beta_j \in \mathbb{R}, \beta_j > 0, j = 1)$	Unstable
Case 4a	$\pm\alpha_j (\alpha_j \in \mathbb{R}, \alpha_j > 0, j = 1), \pm\sigma \pm i\tau (\sigma, \tau \in \mathbb{R}, \sigma > 0, \tau > 0)$	Unstable
Case 4b	$\pm\alpha_j (\alpha_j \in \mathbb{R}, \alpha_j > 0, j = \{1, 2, 3\})$	Unstable
Case 5	$\pm i\beta_j (\beta_j \in \mathbb{R}, \beta_j > 0, j = 1), \pm\sigma \pm i\tau (\sigma, \tau \in \mathbb{R}, \sigma > 0, \tau > 0)$	Unstable

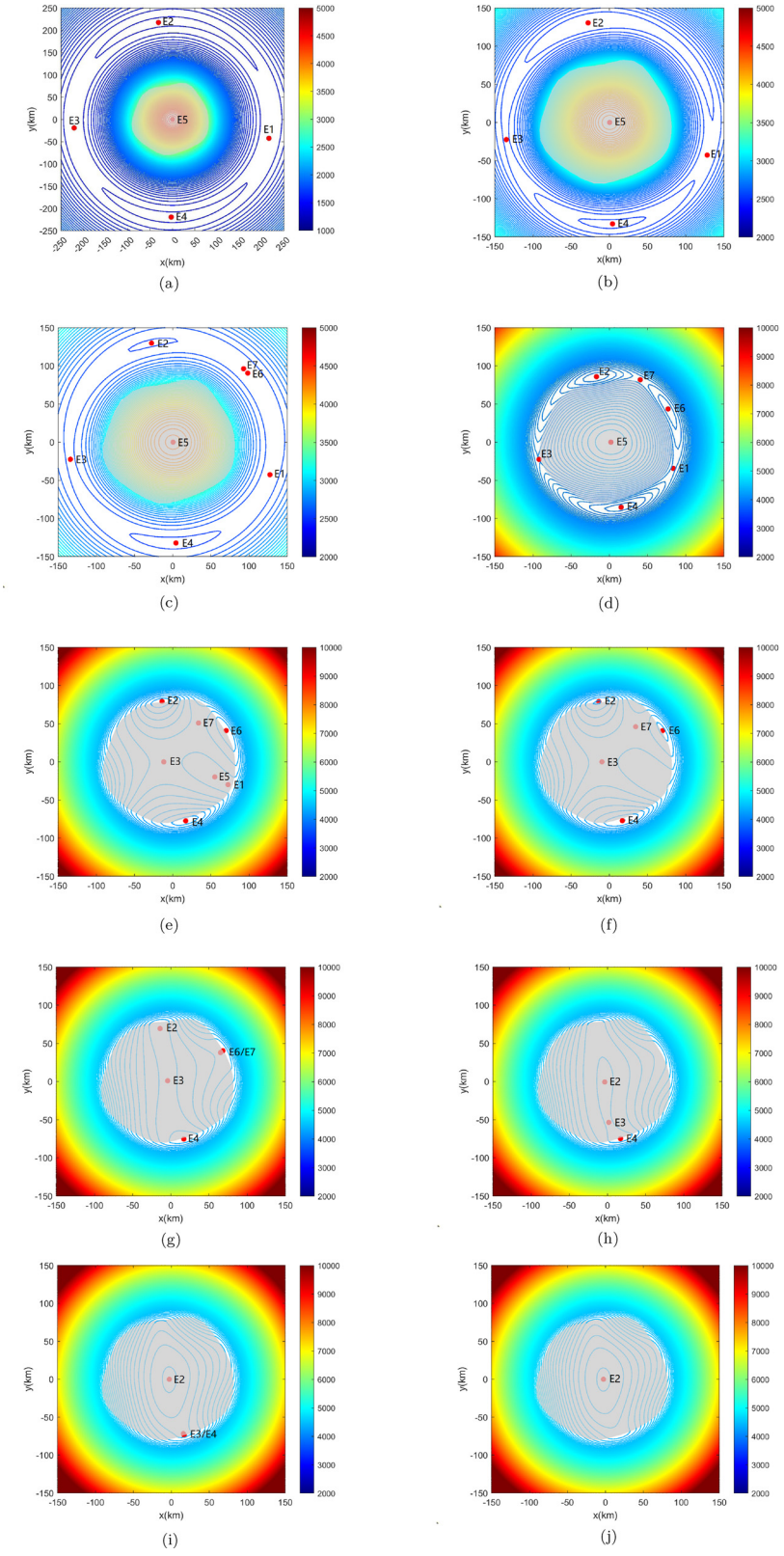

Figure 5: Some typical locations of equilibrium points of asteroid Minerva when increasing the spin speed. (a) $\omega = 0.5\omega_0$. (b) $\omega = 1.06\omega_0$. (c) $\omega = 1.07\omega_0$. (d) $\omega = 2.0\omega_0$. (e) $\omega = 2.27\omega_0$. (f) $\omega = 2.28\omega_0$. (g) $\omega = 2.35\omega_0$. (h) $\omega = 2.37\omega_0$. (i) $\omega = 2.41\omega_0$. (j) $\omega = 2.42\omega_0$.

Table 4: The trend of the equilibrium points number of ten asteroids when the spin speed increases

Serial number	Asteroids	Diameters (km)	Number trend
1	216Kleopatra	217 × 94 × 81	7 → 5 → 3 → 1
2	243Ida	59.8 × 25.4 × 18.6	5 → 3 → 1
3	951Gaspra	18.2 × 10.5 × 8.9	5 → 3 → 1
4	1620Geographos	5.39 × 2.40 × 2.02	5 → 3 → 1
5	2063Bacchus	1.11 × 0.53 × 0.50	5 → 7 → 5 → 3 → 1
6	2867Steins	6.67 × 5.81 × 4.47	5 → 3 → 1
7	6489Golevka	0.75 × 0.55 × 0.59	5 → 3 → 1
8	101955Bennu	0.58 × 0.44 × 0.53	9 → 7 → 5 → 3 → 1
9	S16Prometheus	148 × 93 × 72	5 → 3 → 1
10	1P/Halley	16.8 × 8.77 × 7.76	5 → 7 → 5 → 3 → 1

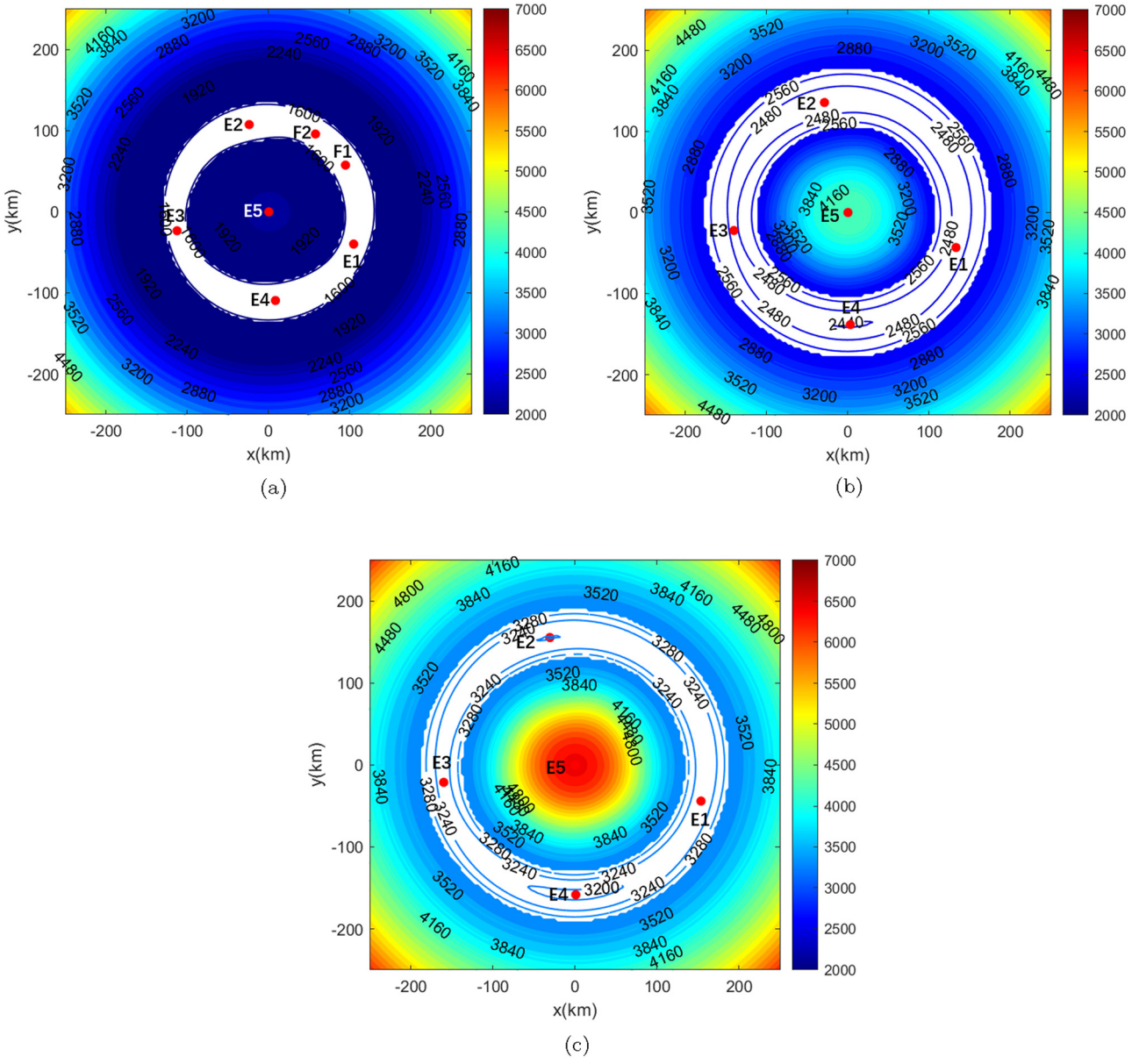

Figure 6: The projection of the equilibrium points of asteroid Minerva in the $+z$ view and the contour map of the zero-velocity surface under different densities. (a) $\rho = 0.5\rho_0$. (b) $\rho = 1.0\rho_0$. (c) $\rho = 1.5\rho_0$.

will be nearly uniformly distributed. As ω increases to $2.27\omega_0$, E1, E3, and E7 come into the body, E3 moves to the center, and E1 and E5 move toward each other. When ω increases to $2.28\omega_0$, E1 and E5 collide and annihilate each other. Then there are five equilibrium points left, which are E2, E3, E4, E6, and E7, and only E3 and E7 are inside the body.

As the spin speed continues to vary, E6 and E7 move toward each other, and the second annihilation occurs; meanwhile, E2 comes into the body. When ω varies from $2.37\omega_0$ to $2.41\omega_0$, E3 and E4 move toward each other, and E2 moves to the center. When ω increases to $2.42\omega_0$, E3 and E4 collide and annihilate each other. After the third annihilation, only equilibrium point E2 is left inside of the body.

Jiang and Baoyin (2018) discussed the annihilation of relative equilibrium points in the gravitational field of irregular-shaped asteroids. Ten asteroids were been simulated, and the results are presented in Table 4. When the spin speed increases, the number of equilibrium points will only decrease in most asteroids, but 2063 Bacchus and 1682 Q1 Halley will increase first and then decrease, which is similar to Minerva.

3.2 The change of density

Then, we considered the change of the equilibrium points during density changes and we defined the initial density $\rho_0 = 1.75$ g cm^{-3}. We kept the spin speed constant and changed the density to $\rho = 0.5\rho_0$ and $\rho = 1.5\rho_0$. The calculation results are shown in Figure 6. Eigenvalues of equilibrium points at different densities are shown in Tables 5 and 6. At the same time, Table 7 presents the topological cases of the equilibrium points under the three densities.

As shown in Figure 6 and Table 7 that when $\rho = 1.5\rho_0$, the number of equilibrium points and their topological cases did not change, the location distribution is close to that when $\rho = 1.0\rho_0$. However, when $\rho = 0.5\rho_0$, the number of equilibrium points increased to seven, as shown in Figure 6(a), and F1 and F2 are newly appeared equilibrium points. The positions of F1 and F2 are located between E1 and E2. Also, the topological cases of each equilibrium points are also changed. The topological cases of E2 and E4 are case 4a, the topological case of F1 is case 1, and the topological case of F2 is case 2.

4 Simulation of the moonlet orbits

Asteroid Minerva has two small moonlets: Aegis and Gorgoneion. Their semi-major axes of rotation around the primary asteroid are 623.5 and 375 km (Marchis *et al*. 2013). To understand the small moonlets motion under Minerva's gravitational potential, we simulated the motion of Gorgoneion. Since Aegis is too far from Minerva, the motion of Gorgoneion is more meaningful to research.

Figure 7 shows the simulation of the Gorgoneion's orbit under the Minerva gravitational potential. Figure 7(a) shows 3D maps of the orbits relative to the body-fixed coordinate system, and Figure 7(b) shows 3D maps of the orbits relative to the equatorial inertial coordinate system. At the initial moment of the orbit simulation, the position is located on the x-axis, and the initial semi-major axis is 375 km, which is equal to the semi-major axis of Gorgoneion. The simulation time is 598.2 h, which means, that when Minerva rotates 100 times, the orbit simulation ends. Figure 7(c) presents the mechanical energy of the orbit, while Figure 7(d) presents the Jacobian integral of the orbit. The mechanical energy of the orbit varies periodically between −270.0 and −267.5 J/kg, and the Jacobian integral of the orbit is approximately constant. The results show that its value is about −2954.4 J/kg. As shown in Figure 8, the semi-major axis of the track changes periodically, the eccentricity is about 0.096 to 0.106, and the median value is around 0.1. The inclination of the orbit relative to the equatorial plane of Minerva is about 17.25°.

Table 5: Eigenvalues of the equilibrium points around Minerva when $\rho = 1.5\rho_0$

Equilibrium points	λ_1	λ_2	λ_3	λ_4	λ_5	λ_6
E1	0.000299i	−0.000299i	0.000296i	−0.000296i	0.000080	−0.000080
E2	0.000299i	−0.000299i	0.000264i	−0.000264i	0.000104i	−0.000104i
E3	0.000306i	−0.000306i	0.000294i	−0.000294i	0.000097	−0.000097
E4	0.000297i	−0.000297i	0.000266i	−0.000266i	0.000104i	−0.000104i
E5	0.001114i	−0.001114i	0.000923i	−0.000923i	0.000529i	−0.000529i

Table 6: Eigenvalues of the equilibrium points around Minerva when $\rho = 0.5\rho_0$

Equilibrium points	λ_1	λ_2	λ_3	λ_4	λ_5	λ_6
E1	$0.000313i$	$-0.000313i$	$0.000302i$	$-0.000302i$	0.000137	−0.000137
E2	$-0.000084 + 0.000210i$	$-0.000084 - 0.000210i$	$-0.000084 + 0.000210i$	$-0.000084 - 0.000210i$	$0.000310i$	$-0.000310i$
E3	$0.000330i$	$-0.000330i$	$0.000303i$	$-0.000303i$	0.000174	−0.000174
E4	$-0.000024 + 0.000199i$	$-0.000024 - 0.000199i$	$-0.000024 + 0.000199i$	$-0.000024 - 0.000199i$	$0.000303i$	$-0.000303i$
E5	$0.000766i$	$-0.000766i$	$0.000533i$	$-0.000533i$	0.000182	−0.000182
F1	$0.000305i$	$-0.000305i$	$0.000248i$	$-0.000248i$	$0.000125i$	$-0.000125i$
F2	$0.000311i$	$-0.000311i$	$0.000303i$	$-0.000303i$	0.000137	−0.000137

Our results show the existence of stable orbits in the gravitational potential of Minerva. When the orbit semi-major axis is the same as Gorgoneion and the eccentricity is about 0.1, then there will be at least one stable orbit exists around Minerva. Through the previous research, when the particle moves near the equilibrium points, the value of the effective potential will change significantly (Jiang 2018). We can see from the figure of effective potential shown in Section 2, it is relatively difficult to obtain a stable periodic orbit around the equilibrium points. Therefore, if we want the irregular shape of Minerva to have less perturbation to the particle's orbit, the particle should move away from the equilibrium points. For Minerva, the four external equilibrium points are all located close to 150 km from the centroid of the asteroid. In Figure 9, we simulated the orbits at different initial distances, we can see that when the initial distance is 150 or 180 km, the orbits are unstable, but when the initial distance is 200 or 300 km the orbits are stable. So to maintain the stability of the orbits, the distance of the orbit relative to the centroid of the asteroid should be much more than 150 km.

5 Conclusion

In this article, we established a three-dimensional model of the asteroid 93 Minerva using the irregular shape model from observations. On the basis of this model, we calculated the physical size of asteroid Minerva to be 182.96 km × 164.37 km × 143.79 km, and the mass to be 3.3603×10^{18} kg, the surface height to be in the range of 63.7 to 93.1 km. Its shape is approximately spherical, and the surface has four significantly convex areas and six significantly concave areas. We recognized five equilibrium points around the Minerva, four of which are external and one is internal. After linearizing these motion equations in the neighborhood of each equilibrium point, we obtained the relevant characteristic equations and analyze the stability of these equilibrium points based on the solutions of the equations. Through the analysis to the eigenvalues of the equilibrium points, the topological cases of the equilibrium points E1–E4 are Case 2, Case 1, Case 2, and Case 1. Specifically, E2 and E4 are stable and are near the y-axis, and E1 and E3 are unstable and are near the x-axis.

We studied the changing trend of equilibrium points by changing the spin speed and density of the Minerva. Keeping the density of Minerva constant and increasing its spin speed gradually and the number of equilibrium points will first increase from five to seven, then the

Table 7: Equilibrium points topological cases around Minerva at different densities

Density	E1	E2	E3	E4	E5	F1	F2
$\rho = 0.5\rho_0$	Case 2	Case 4a	Case 2	Case 4a	Case 1	Case 1	Case 2
$\rho = 1.0\rho_0$	Case 2	Case 1	Case 2	Case 1	Case 1	—	—
$\rho = 1.5\rho_0$	Case 2	Case 1	Case 2	Case 1	Case 1	—	—

annihilations occur, two equilibrium points collide and annihilate each other, the number of equilibrium points will decrease to one finally. When the spin speed is constant and the density changed, and $\rho = 1.5\rho_0$, the positions of the equilibrium points changed locally, and neither the number nor the topological cases changed. When $\rho = 0.5\rho_0$, and the number of equilibrium points increases to seven, and its positions and topological cases also changed, which has a certain impact on its stability. We calculated the gravitational field of Minerva using irregular shape model from observations. What's more, we simulated the orbits of the small moonlet under the gravitational

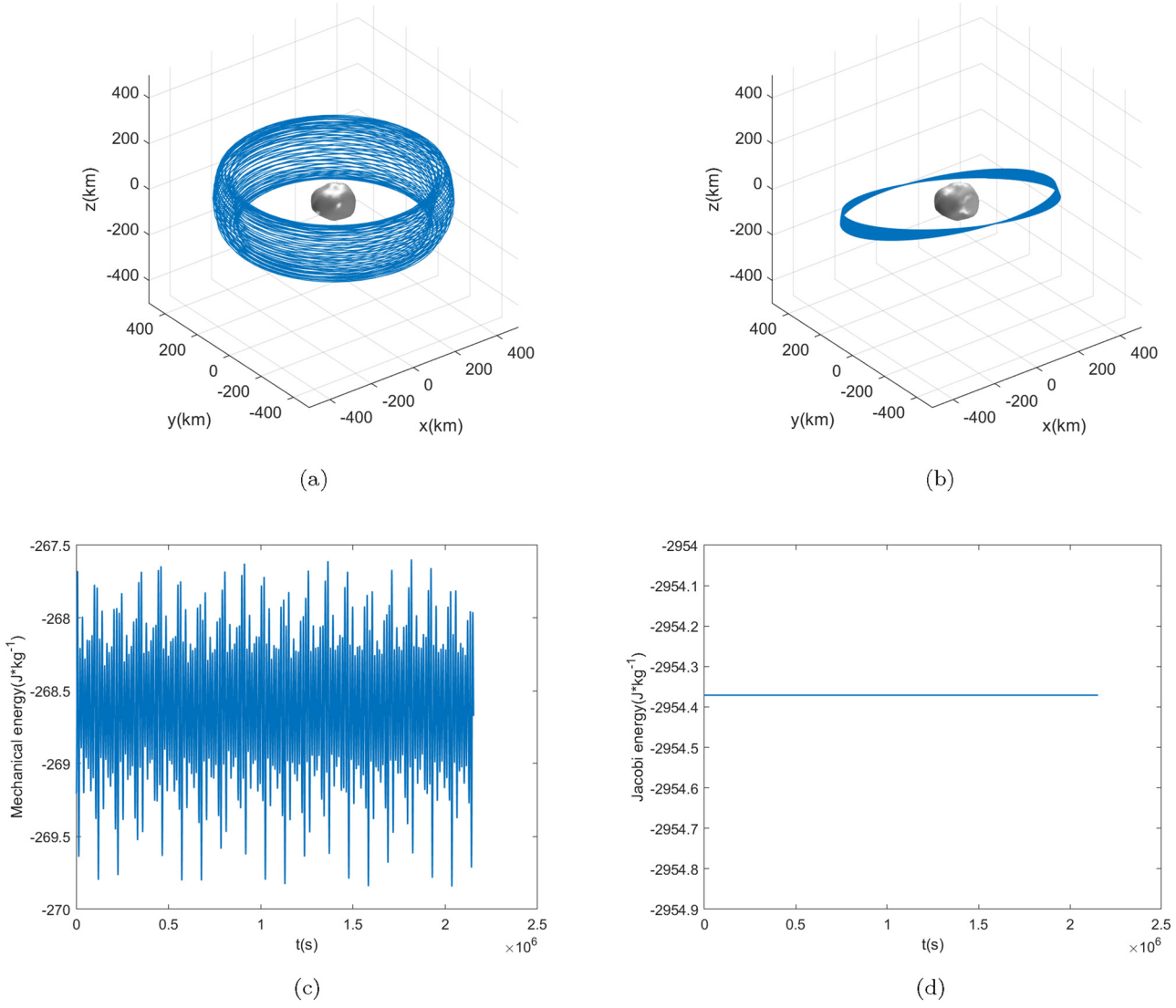

Figure 7: Orbit simulation of Minerva moonlet. (a) 3D map of the orbit in the body-fixed coordinate system. (b) 3D map of the orbit in the inertial system. (c) Mechanical energy of the orbit. (d) Jacobian integral of orbits.

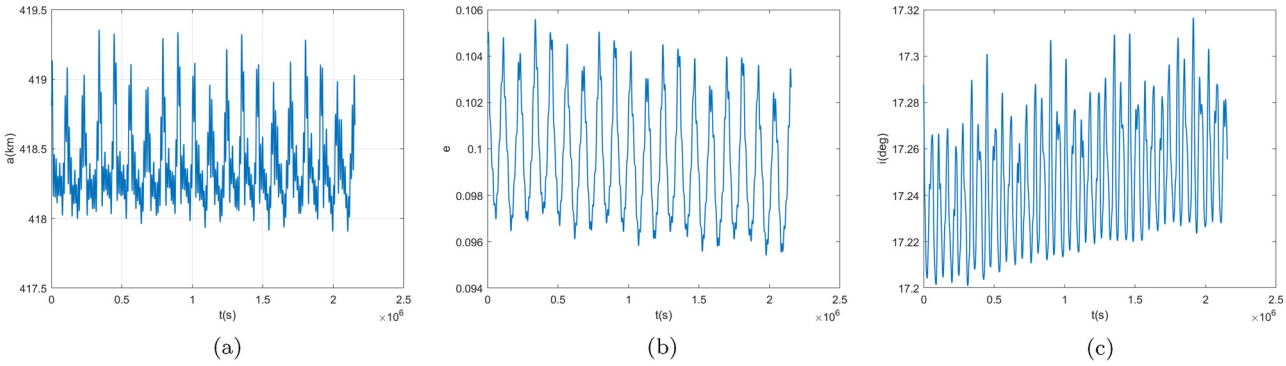

Figure 8: The orbital elements of simulation. (a) The semi-major axis. (b) The eccentricity. (c) The inclination of the orbit relative to the equatorial plane of Minerva.

potential of Minerva. The mechanical energy of the moonlet's orbit changes periodically and the Jacobian integral remains conservative. The result shows that there are stable orbits exist in the Minerva system. Through the simulation of Minerva, we research its characteristics and orbits, which will help to carry out explorations in the future.

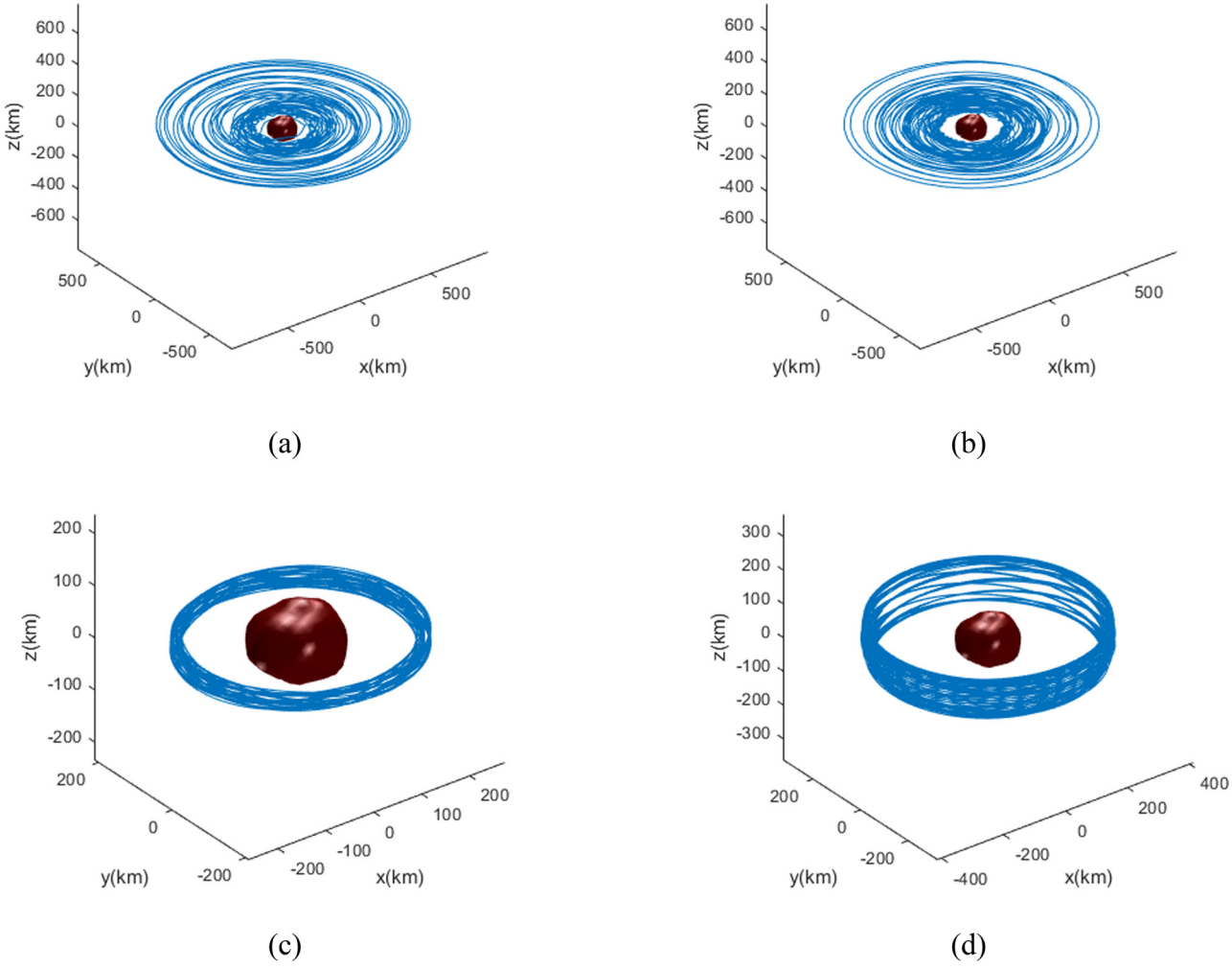

Figure 9: Orbits around Minerva in different initial distances (*d*: initial distance). (a) d = 150 km. (b) d = 180 km. (c) d = 200 km. (d) d = 300 km.

Acknowledgments: We gratefully acknowledge the reviewers for their helpful and constructive suggestions that helped us substantially improve the article.

Funding information: This work was supported by the Natural Science Foundation of China (No. U21B2050, No. 11902238) and the China Postdoctoral Science Foundation funded project (No. 2020M673373). All contributions by the co-author XiaoDuan Zou are not funded by NASA or any Chinese agency.

Author contributions: H.L.: conceptualization, methodology, software, validation, data curation, writing-original draft, visualization, and project administration; Y.J.: conceptualization, methodology, software, validation, supervision, project administration, and funding acquisition; A.L.: conceptualization, methodology, formal analysis, data curation, writing-original draft, supervision, and project administration; Y.W.: software, formal analysis, resources, writing-original draft, and visualization; X.Z.: writing-review and editing; J.P.: resources and writing-review and editing; Y.C.: formal analysis and writing-original draft; Y.Y.: resources and writing-review and editing; C.Z.: resources and writing-review and editing; Y.L.: resources and writing-review and editing; J.C.: resources and writing-review and editing.

Conflict of interest: The authors declare no conflict of interest.

References

Abe S, Mukai T, Hirata N, Barnouin-Jha OS, Cheng AF, Demura H, et al. 2006. Mass and local topography measurements of Itokawa by Hayabusa. Science. 312(5778):1344–1347.

Aljbaae S, Chanut TG, Prado AF, Carruba V, Hussmann H, Souchay J, et al. 2019. Orbital stability near the (87) Sylvia system. Mon Not R Astron Soc. 486(2):2557–2569.

Barucci M, Fulchignoni M, Rossi A. 2007. Rosetta asteroid targets: 2867 Steins and 21 Lutetia. Space Sci Rev. 128(1):67–78.

Belton M, Veverka J, Thomas P, Helfenstein P, Simonelli D, Chapman C, et al. 1992. Galileo encounter with 951 Gaspra: First pictures of an asteroid. Science. 257(5077):1647–1652.

Chanut T, Winter O, Amarante A, Araújo N. 2015. 3D plausible orbital stability close to asteroid (216) Kleopatra. Mon Not R Astron Soc. 452(2):1316–1327.

Fujiwara A, Kawaguchi J, Yeomans D, Abe M, Mukai T, Okada T, et al. 2006. The rubble-pile asteroid Itokawa as observed by Hayabusa. Science. 312(5778):1330–1334.

Huang J, Ji J, Ye P, Wang X, Yan J, Meng L, et al. 2013. The ginger-shaped asteroid 4179 Toutatis: new observations from a successful flyby of changae-2. Sci Rep. 3(1):1–6.

Ji J, Jiang Y, Zhao Y, Wang S, Yu L. 2015. Chang'e-2 spacecraft observations of asteroid 4179 toutatis. Proc Int Astron Union. 10(S318):144–152.

Jiang Y. 2015. Equilibrium points and periodic orbits in the vicinity of asteroids with an application to 216 Kleopatra. Earth, Moon, and Planets. 115(1):31–44.

Jiang Y. 2018. Dynamical environment in the vicinity of asteroids with an application to 41 Daphne. Results Phys. 9:1511–1520.

Jiang Y. 2019. Dynamical environment in the triple asteroid system 87 Sylvia. Astrophys Space Sci. 364(4):1–12.

Jiang Y, Baoyin H. 2016. Periodic orbit families in the gravitational field of irregular-shaped bodies. Astron J. 152(5):137.

Jiang Y, Baoyin H. 2018. Annihilation of relative equilibria in the gravitational field of irregular-shaped minor celestial bodies. Planet Space Sci. 161:107–136.

Jiang Y, Baoyin H, Li H. 2015. Periodic motion near the surface of asteroids. Astrophys Space Sci. 360(2):1–10.

Jiang Y, Baoyin H, Li H. 2018. Orbital stability close to asteroid 624 Hektor using the polyhedral model. Adv Space Res. 61(5):1371–1385.

Jiang Y, Baoyin H, Li J, Li H. 2014. Orbits and manifolds near the equilibrium points around a rotating asteroid. Astrophys Space Sci. 349(1):83–106.

Jiang Y, Baoyin H, Wang X, Yu Y, Li H, Peng C, et al. 2016. Order and chaos near equilibrium points in the potential of rotating highly irregular-shaped celestial bodies. Nonlinear Dyn. 83(1):231–252.

Jiang Y, Li H. 2019. Equilibria and orbits in the dynamical environment of asteroid 22 Kalliope. Open Astron. 28(1):154–164.

Jiang Y, Liu X. 2019. Equilibria and orbits around asteroid using the polyhedral model. New Astron. 69:8–20.

Lazzaro D, Angeli C, Carvano J, Mothé-Diniz T, Duffard R, Florczak M. 2004. S3os2: The visible spectroscopic survey of 820 asteroids. Icarus. 172(1):179–220.

Marchis F, Descamps P, Hestroffer D, Berthier J, Vachier F, Boccaletti A, et al. 2003. A three-dimensional solution for the orbit of the asteroidal satellite of 22 Kalliope. Icarus. 165(1):112–120.

Marchis F, Macomber B, Berthier J, Vachier F, Emery J. 2009. S/2009 (93) 1 and S/2009 (93) 2. Int Astron Union Circular. 9069:1.

Marchis F, Vachier F, Ďurech J, Enriquez J, Harris A, Dalba P, et al. 2013. Characteristics and large bulk density of the c-type main-belt triple asteroid (93) Minerva. Icarus. 224(1):178–191.

Mota ML, Rocco EM. 2019. Equilibrium points stability analysis for theasteroid 21 lutetia. In: Journal of Physics: Conference Series. Vol. 1365. IOP Publishing. p. 012007.

Moura T, Winter O, Amarante A, Sfair R, Borderes-Motta G, Valvano G. 2020. Dynamical environment and surface characteristics of asteroid (16) Psyche. Mon Not R Astron Soc. 491(3):3120–3136.

Price SD, Egan MP, Carey SJ, Mizuno DR, Kuchar TA. 2001. Midcourse space experiment survey of the galactic plane. Astron J. 121(5):2819.

Ryan EL, Woodward CE. 2010. Rectified asteroid albedos and diameters from iras and msx photometry catalogs. Astron J. 140(4):933.

Scheeres DJ, Ostro SJ, Hudson R, Werner RA. 1996. Orbits close to asteroid 4769 Castalia. Icarus. 121(1):67–87.

Tedesco EF, Noah PV, Noah M, Price SD. 2002. The supplemental IRAS minor planet survey. Astron J. 123(2):1056.

Usui F, Kuroda D, Müller TG, Hasegawa S, Ishiguro M, Ootsubo T, et al. 2011. Asteroid catalog using AKARI: AKARI/IRC mid-infrared asteroid survey. Publ Astron Soc Jpn. 63(5):1117–1138.

Veverka J, Robinson M, Thomas P, Murchie S, Bell III J, Izenberg N, et al. 2000. NEAR at Eros Imaging and spectral results. Science. 289(5487):2088–2097.

Veverka J, Thomas P, Harch A, Clark B, Bell III J, Carcich B, et al. 1997. NEAR's flyby of 253 mathilde: Images of a C asteroid. Science. 278(5346):2109–2114.

Wang X, Jiang Y, Gong S. 2014. Analysis of the potential field and equilibrium points of irregular-shaped minor celestial bodies. Astrophys Space Sci. 353(1):105–121.

Werner RA, Scheeres DJ. 1996. Exterior gravitation of a polyhedron derived and compared with harmonic and mascon gravitation representations of asteroid 4769 Castalia. Celest Mech Dyn Astron. 65(3):313–344.

Yang B, Wahhaj Z, Beauvalet L, Marchis F, Dumas C, Marsset M, et al. 2016. Extreme ao observations of two triple asteroid systems with sphere. Astrophys J Lett. 820(2):L35.

Yu Y, Baoyin H. 2012a. Generating families of 3D periodic orbits about asteroids. Mon Not R Astron Soc. 427(1):872–881.

Yu Y, Baoyin H. 2012b. Orbital dynamics in the vicinity of asteroid 216 Kleopatra. Astron J. 143(3):62.

Zhao Y, Wang S, Hu S, Ji J. 2013. A research on imaging strategy and imaging simulation of toutatis in the Chang'e 2 flyby mission. Acta Astron Sin. 54(5):447–454.

Zou X, Li C, Liu J, Wang W, Li H, Ping J. 2014. The preliminary analysis of the 4179 Toutatis snapshots of the Changae-2 flyby. Icarus. 229:348–354.

Appendix

The detailed calculation of the equilibrium points eigenvalues.

The linearized equation of motion of the massless particle relative to the equilibrium point can be written as equation (A1). The characteristic equation of the equation (A4) could be satisfied as equation (A5). Through the calculation, we can obtain the eigenvalues of the equilibrium points.

$$\mathbf{M}\ddot{\mathbf{X}} + \mathbf{G}\dot{\mathbf{X}} + \mathbf{K}\mathbf{X} = 0, \tag{A1}$$

$$\mathbf{X} = \begin{bmatrix} \xi \\ \eta \\ \zeta \end{bmatrix} = \begin{bmatrix} x - x_L \\ y - y_L \\ z - z_L \end{bmatrix}, \tag{A2}$$

$$\mathbf{M} = \begin{pmatrix} 1 & 0 & 0 \\ 0 & 1 & 0 \\ 0 & 0 & 1 \end{pmatrix}, \quad \mathbf{G} = \begin{pmatrix} 0 & -2\omega & 0 \\ 2\omega & 0 & 0 \\ 0 & 0 & 0 \end{pmatrix}, \quad \mathbf{K} = \begin{pmatrix} V_{xx} & V_{xy} & V_{xz} \\ V_{xy} & V_{yy} & V_{yz} \\ V_{xz} & V_{yz} & V_{zz} \end{pmatrix}, \tag{A3}$$

$$\frac{\mathrm{d}^2}{\mathrm{d}t^2}\begin{bmatrix} \xi \\ \eta \\ \zeta \end{bmatrix} + \begin{pmatrix} 0 & -2\omega & 0 \\ 2\omega & 0 & 0 \\ 0 & 0 & 0 \end{pmatrix} \cdot \frac{\mathrm{d}}{\mathrm{d}t}\begin{bmatrix} \xi \\ \eta \\ \zeta \end{bmatrix} + \begin{pmatrix} V_{xx} & V_{xy} & V_{xz} \\ V_{xy} & V_{yy} & V_{yz} \\ V_{xz} & V_{yz} & V_{zz} \end{pmatrix} \cdot \begin{bmatrix} \xi \\ \eta \\ \zeta \end{bmatrix} = 0, \tag{A4}$$

$$\begin{vmatrix} \lambda^2 + V_{xx} & -2\omega\lambda + V_{xy} & V_{xz} \\ 2\omega\lambda + V_{xy} & \lambda^2 + V_{yy} & V_{yz} \\ V_{xz} & V_{yz} & \lambda^2 + V_{zz} \end{vmatrix} = 0. \tag{A5}$$

In the aforementioned expression:

$$V_{xx} = \left(\frac{\partial^2 V}{\partial x^2}\right)_{\mathrm{L}} \quad V_{xy} = \left(\frac{\partial^2 V}{\partial x \partial y}\right)_{\mathrm{L}}$$
$$V_{yy} = \left(\frac{\partial^2 V}{\partial y^2}\right)_{\mathrm{L}} \quad V_{yz} = \left(\frac{\partial^2 V}{\partial y \partial z}\right)_{\mathrm{L}} \tag{A6}$$
$$V_{zz} = \left(\frac{\partial^2 V}{\partial z^2}\right)_{\mathrm{L}} \quad V_{xz} = \left(\frac{\partial^2 V}{\partial x \partial z}\right)_{\mathrm{L}}.$$